



# Ezurpimtrostat, A Palmitoyl-Protein Thioesterase-1 Inhibitor, Combined with PD-1 Inhibition Provides CD8<sup>+</sup> Lymphocyte Repopulation in Hepatocellular Carcinoma

Eloïne Bestion<sup>1</sup> · Madani Rachid<sup>1</sup> · Annemiläi Tijeras-Raballand<sup>2</sup> · Gael Roth<sup>3</sup> · Thomas Decaens<sup>3</sup> · Christelle Analdi<sup>1</sup> · Soraya Mezouar<sup>1,4</sup> · Eric Raymond<sup>1,5</sup> · Philippe Halfon<sup>1</sup>

Accepted: 20 November 2023

© The Author(s), under exclusive licence to Springer Nature Switzerland AG 2023

## Abstract

**Background** Palmitoyl-protein thioesterase-1 (PPT1) is a clinical stage druggable target for inhibiting autophagy in cancer. **Objective** We aimed to determine the cellular and molecular activity of targeting PPT1 using ezurpimtrostat, in combination with an anti-PD-1 antibody.

**Methods** In this study we used a transgenic immunocompetent mouse model of hepatocellular carcinoma.

**Results** Herein, we revealed that inhibition of PPT1 using ezurpimtrostat decreased the liver tumor burden in a mouse model of hepatocellular carcinoma by inducing the penetration of lymphocytes into tumors when combined with anti-programmed death-1 (PD-1). Inhibition of PPT1 potentiates the effects of anti-PD-1 immunotherapy by increasing the expression of major histocompatibility complex (MHC)-I at the surface of liver cancer cells and modulates immunity through recolonization and activation of cytotoxic CD8<sup>+</sup> lymphocytes.

**Conclusions** Ezurpimtrostat turns cold tumors into hot tumors and, thus, could improve T cell-mediated immunotherapies in liver cancer.

---

Eloïne Bestion, Madani Rachid, Annemiläi Tijeras-Raballand, Soraya Mezouar, Eric Raymond, Philippe Halfon have contributed equally.

✉ Philippe Halfon  
phalfon@genosciencepharma.com

<sup>1</sup> Genoscience Pharma, 10, Rue d'Iéna, 13006 Marseille, France

<sup>2</sup> AFR Oncologie, Boulogne-Billancourt, France

<sup>3</sup> Centre hospitalouniversitaire Grenoble Alpes/Institute for Advanced Biosciences, Centre national de la recherche scientifique, Unité mixte de recherche 5309-Institut national de la santé et de la recherche médicale U1209, University Grenoble Alpes/Hepato-Gastroenterology and Digestive Oncology Department, 38043 Grenoble, France

<sup>4</sup> Etablissement français du sang, Centre national de la recherche scientifique, Anthropologie bio-culturelle, droit, éthique et santé, “Biologie des Groupes Sanguins”, Aix-Marseille University, Marseille, France

<sup>5</sup> Oncology Department, Groupe Hospitalier Paris Saint Joseph, Paris, France

## Key Points

Inhibition of palmitoyl-protein thioesterase-1 (PPT1) enhances the antitumor activity of anti-programmed death-1 (PD-1) in liver cancer in a preclinical model.

This study provides a rationale for the use of this combination in clinical cancer trials.

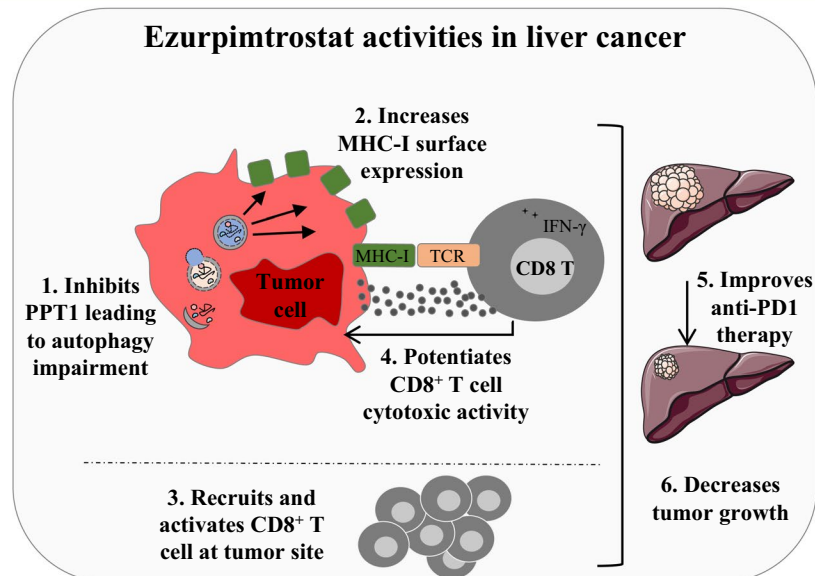
## Graphical Abstract

# Targeted Oncology

 PEER-REVIEWED  
FEATURE

**Ezurpimtrostat, a palmitoyl-protein thioesterase-1 inhibitor, combined with PD-1 inhibition provides CD8<sup>+</sup> lymphocyte repopulation in hepatocellular carcinoma**

Eloïne Bestion, Madani Rachid, Annemiläi Tijeras-Raballand, Gael Roth, Thomas Decaens, Christelle Ansaldi, Soraya Mezouar, Eric Raymond, Philippe Halfon



This graphical abstract represents the opinions of the authors. For a full list of declarations, including funding and author disclosure statements, and copyright information, please see the full text online.

## 1 Introduction

PPT1 (palmitoyl-protein thioesterase-1) is a lysosomal enzyme that plays a central role in the hydrolysis of palmitoylated proteins [1]. PPT1 deficiency can be induced by knocking down gene functions in preclinical models, and it is also caused by a human mutation in neuronal ceroid lipofuscinosis-1, which leads to abnormal accumulation of unfolded palmitoylated proteins, resulting in neurodegeneration [1, 2]. PPT1-dependent depalmitoylation is involved in the stabilization of lysosomal localization of v-ATPase subunits needed to maintain lysosomal acidity and to facilitate mTOR localization and subsequent activation [3–5]. In cancer cells, the recycling of proteins through lysosomes plays an important role in sustaining

signaling without inducing the accumulation of unusable proteins that may trigger autophagy and apoptosis. Normalizing palmitoyl function using enzymatic inhibitors that balance high levels of palmitoylation may be desirable for impairing enhanced oncogenic cell signaling [6]. Improved knowledge of PPT1 three-dimensional protein conformation and enzymatic substrates has led to the development of allosteric and substrate-competitive inhibitors. DQ661 and didemnin B have shown that PPT1 inhibition causes both the disruption of lysosome function and accumulation of excess proteins, which in turn are associated with antitumor activity [7–10]. In melanoma models, the inhibition of PPT1 was found to increase anti-PD-1 anti-tumor activity and was associated with CD8<sup>+</sup> T cell tumor colonization, proliferation, and activation

involved in tumor cell death, thereby enhancing the anti-tumor efficacy of programmed death-1 (PD-1) inhibitors [11]. Increasing evidence suggests that autophagy can induce immune checkpoint protein (PD-L1 and MHC-I/II) degradation in cancer cells [12, 13], which plays an important role in regulating cancer cell immune escape. In addition to the autophagic degradation of immune checkpoint proteins, autophagy induction in immune cells (macrophages and dendritic cells) manipulates antigen presentation and T cell activity. These reports suggested that targeting autophagy can positively regulate the immune escape of cancer cells.

Ezurpimtrostat/GNS561 is a small lysosomotropic basic lipophilic clinical-stage molecule that acts as a potent PPT1 inhibitor. Several studies have highlighted the importance of ezurpimtrostat in cancer treatment by blocking PPT1-dependent autophagic activity [9, 14, 15]. We have previously reported the mechanism of action of ezurpimtrostat, including lysosomal permeabilization, autophagy inhibition, and mTOR inhibition. Treatment of PPT1 siRNA-transfected cells with ezurpimtrostat failed to enhance lipidated LC3, reflecting autophagy inhibition and antitumor activity, depicting PPT1 as the molecular target of ezurpimtrostat.

In this study, we investigated the effects of PPT1 inhibition by ezurpimtrostat on PD-1 inhibitors in a transgenic immunocompetent hepatocellular carcinoma (HCC) mouse model. This study provides evidence that the inhibition of PPT1 sensitizes tumors to immunotherapy, highlighting the clinical rationale for combining PPT1 and PD-1 inhibitors in cancer treatment.

## 2 Methods

### 2.1 Mouse Model and Treatment

Seven-week-old transgenic C57BL6/ASV-B male mice that develop HCC as previously described were obtained from TAAM UAR44 (CNRS, Orléans) [16]. Briefly, precise targeting of the SV40 T early region in the liver of transgenic mice was achieved using 700 base pairs of antithrombin regulatory sequences to control oncogene expression. Hepatocyte hyperplasia/dysplasia occurred at 8 weeks (W), nodules corresponding to the adenomatous stage were observed at W12, and diffuse HCC was observed at W16. HCC progression is also characterized by angiogenesis and severe vessel anomalies, such as capillarization and arterialization. All experiments were performed following Directive 2010/63/EU of the European Parliament and Council on 22 September 2010. This project was approved by the local ethic committee (Comité d'éthique en experimentation animale Lariboisière-85 Villemin n°9).

Before the experiment, a control ultrasound procedure was performed to homogeneously allocate the animals at 8 weeks of age on the basis of liver volume. As illustrated in Fig. 1, the study design included the following groups: vehicle (control group), ezurpimtrostat, anti-PD-1 (CVP033, CrownBio), and a combination group (ezurpimtrostat with anti-PD-1). For ezurpimtrostat (alone or in combination, 50 mg/kg) and vehicle, mice were treated daily for 6 days/week, at a constant dosage of 10 mL/kg per os. Anti-PD-1 was diluted in phosphate-buffered saline (PBS; Life Technologies, L0615-500) extemporaneously, before administration. Mice receiving anti-PD-1 (alone or in combination, 10 mg/kg) were treated twice a week at a constant dose of 10 mL/kg via intraperitoneal injection. All mice were weighed three times per week to adjust the treatment volume.

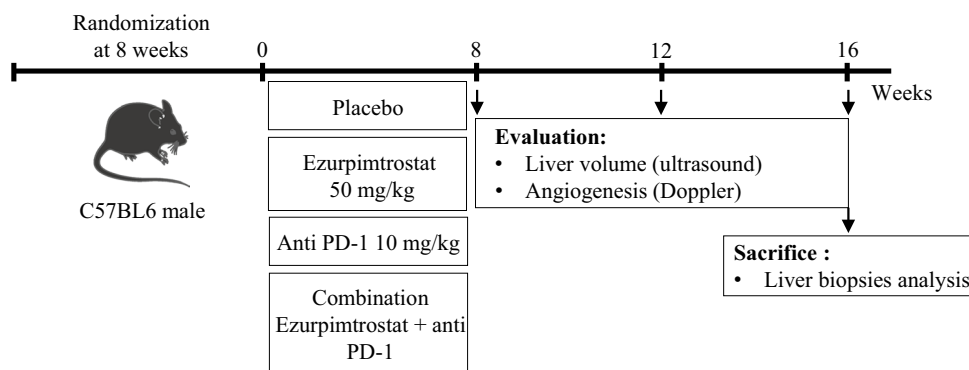


**Fig. 1** Study design. Four groups of mice ( $n = 10$ ) were treated for 8 weeks with ezurpimtrostat (10 mg/kg, 6× per week, per os), anti-PD-1 (10 mg/kg, 2× per week, intraperitoneal), ezurpimtrostat (10 mg/kg, 6× per week) plus anti-PD-1 (10 mg/kg, 2× per week, intra-

peritoneal), or vehicle (water at  $\text{pH } 4 \pm 0.2$ , per os) as a control. Every 4 weeks, echography and Doppler were performed to monitor tumor burden. At week 16, the animals were sacrificed, and organs were harvested for preservation

The mice were euthanized at W16, and their livers were collected and weighed, macronodules were counted, and livers were paraffin-embedded for analysis. All treatments were well tolerated on the basis of animal behavior and body weight follow-up (Supplementary Fig. S1). One animal was excluded from the analysis because it died prematurely in the ezurpimtrostat group due to an improper administration of gavage.

## 2.2 Doppler Ultrasound

The Doppler ultrasound assessment of this model has been described previously [17]. In this model, liver tumor angiogenesis has been described to be correlated with blood flow in the celiac trunk (CT). When abnormal angiogenesis is sprayed into the liver, the blood flow increases on CT. Ultrasound imaging was performed every 4 weeks (Fig. 1). The minimum and maximum detectable velocities were approximately 1 and 120 cm/s, respectively.

## 2.3 Immunostaining

Immunohistochemical staining was performed on 5- $\mu$ m-thick slices from paraffin-embedded tumors and counterstained with hematoxylin–phloxin–safron (HES), using an automated immunohistochemical stainer (Tissue-Tek Prisma@Plus, Sakura, France) following the manufacturer's instructions. Immunostaining was performed using an automated immunohistochemical stainer (BondMax; Leica, Wetzlar, Germany). The CD8 antibody (Abcam, #ab209775, 1/200) was used to assess lymphocyte localization in HCC livers at the perinodular and intramodular levels. Immunofluorescence was performed on 5- $\mu$ m-thick sections from the paraffin-embedded tumors. Tissue sections were deparaffinized in xylene baths three times for 5 min each before gradual hydration with ethanol in successive 5-min baths of 2 min each in 100%, 95%, 70%, and 50% ethanol. Tissue sections were rinsed twice for 5 min in phosphate-buffered saline (PBS). Labeling of p62 and PPT1 was preceded by a heat-induced epitope retrieval step to improve the detection of antibody staining in paraffin-embedded tissue sections. The coverslips were placed in boiling antigen retrieval buffer (Tris 10 mM, EDTA 1 mM, Tween 20 0.05% in water, pH 9) for 10 min, and then immersed in cold water to allow the antigenic sites to re-form. The coverslips were washed once in PBS before two permeabilization baths with permeation buffer (Triton 0.4% in PBS) for 10 min at room temperature (RT). The coverslips were washed twice with PBS. For all antibodies, unspecific sites were blocked with a blocking buffer solution [5% fetal bovine serum (FBS, Life Technologies, #10270-098), 0.1% Tween 20 (Biosolve, #20452335) in PBS (Life Technologies, #14200-067)] for 30 min at RT and washed twice. p62 (Abcam, #ab240635,

1/150), MHC-I (BioLegend, #125508, 1/150), PPT1 (Invitrogen, #PA5-29177, 1/220) antibodies, and 4',6-diamidino-2-phenylindole (DAPI, Invitrogen, #D1306, 1/1000) were incubated overnight at 4 °C in the dark. The following day, the coverslips were washed twice with PBS and incubated for 1 h at RT with Alexa647-conjugated anti-rabbit secondary antibody (Invitrogen, #A-31573, 1/500) to detect both p62 and PPT1 proteins. All antibodies were diluted in blocking buffer solution. Labeled cells were washed twice with PBS, mounted using Fluoromount™ Aqueous Mounting medium, and stored overnight at 4 °C before analysis. For image analysis, fluorescence images were acquired using an ApoTome module associated with a Zeiss microscope (Zeiss, Germany) equipped with an AxioCam MRm camera and collected using AxioVision software (Zeiss, Germany) with a 63 $\times$  oil objective. Randomly selected microscopic tiles (5  $\times$  5) were acquired using the Zen 3.0 software (Blue Edition, Zeiss, Germany). Labeled areas from selected fields were quantified using ImageJ.

## 2.4 Cell isolation and cell line culture

The HepG2 (hepatocellular carcinoma, ATCC, #HB-8065) cell line was cultured in low-glucose Dulbecco's modified Eagle medium (DMEM; Thermo Fisher Scientific, #21,885,025) supplemented with 1% penicillin–streptomycin (Dutscher) and 10% fetal bovine serum (FBS) (GE Healthcare, #SV30160.03C). Peripheral blood mononuclear cells (PBMCs) were isolated from buffy coats of healthy donors via density-gradient centrifugation using Ficoll (Eurobio, #CMSMSL01-01) at 800g (brake off) for 30 min at 20 °C. PBMCs were cryopreserved at – 80 °C in 90% FBS (Gibco, #10099141) and 10% dimethyl sulfoxide (DMSO, Sigma-Aldrich, #D2650). Lymphocytes were isolated and purified using a Pan T Cell Isolation Kit (#130-096-535; Miltenyi Biotec). The degree of achieved lymphocyte purity was at least 98%, and it was assessed using standard sorting procedures via flow cytometry.

## 2.5 Flow Cytometry Analysis

IFN- $\gamma$  expression was evaluated in the CD3<sup>+</sup>CD8<sup>+</sup> lymphocyte population co-cultured with HepG2 cells with or without treatment with ezurpimtrostat at 0.6, 6, or 7  $\mu$ M for 24 h. After incubation, the cells were suspended in PBS (Dutscher, #L0615-500) containing 1% FBS and 2 mM EDTA (Dutscher, #P10-15100). Cells were labeled with viability fixable dye (Miltenyi Biotec, #130-109-812), and antibodies against CD3 (Miltenyi Biotec, #130-113-141), CD8 (Miltenyi Biotec, #130-110-681), and IFN- $\gamma$  (BD Pharmingen, #560741).

MHC-1 expression was evaluated in HepG2 cells. Briefly, cells (60,000 cells/well) were seeded in a 96-well tissue culture plate in 90  $\mu$ L DMEM with low glucose. After 24 h of plating, the cultivated cells were treated with increasing concentrations of GNS561 (10  $\mu$ L) or vehicle control and were incubated for an additional 24 h. The cells were harvested, washed, and incubated with the v450 viability stain (Invitrogen, #650863-14), MHC-I (Invitrogen, #65-0863), and NBR1 (Santa Cruz Biotechnology, #sc130380) antibodies.

Labeled cells were acquired from at least 50,000 cells, collected using an Attune NxT flow cytometer (Thermo Fisher Scientific), and analyzed using FlowJo (FlowJo v10.6.2).

## 2.6 Statistical Analysis

Statistical analyses were performed using Prism version 8.4.3. For datasets with a normal distribution, multiple comparisons were performed using a one-way ANOVA with Tukey's post-hoc analysis. An unpaired *t*-test was used to compare two groups of normally distributed data. Data are presented as mean  $\pm$  standard deviation (SD). Statistical significance was defined as a *p*-value  $< 0.05$ .

## 3 Results

### 3.1 PPT1 Inhibition in Combination with Anti-PD-1 Decreases Tumor Growth

As autophagy inhibitors combined with immune checkpoint inhibitors provide opportunities to enhance antitumor activity [11, 18], we investigated the efficacy of ezurpimtrostat in combination with anti-PD-1 in a transgenic immunocompetent HCC mouse model according to the study design described in Fig. 1. Twelve weeks post-treatment, ezurpimtrostat monotherapy or combination therapy with anti-PD-1 led to a significant decrease in liver volume compared to the vehicle control or anti-PD-1 groups (Supplementary Table 1). Moreover, the tumor volume at the end of the experiment (day 16) was significantly smaller in mice treated with ezurpimtrostat monotherapy or combination therapy with anti-PD-1 than that in the vehicle control or anti-PD-1 groups. At both time points, no significant differences were observed between the control and anti-PD-1 treatment groups. As HCC has been reported to be a highly vascular tumor [19], we evaluated blood flow at 12 and 16 weeks. As illustrated in Supplementary Table 1, ezurpimtrostat monotherapy or combination therapy with

anti-PD-1 significantly decreased blood flow compared with the vehicle control, whereas an increase was observed during anti-PD-1 treatment. Interestingly, at the end of the experiment, the combination of ezurpimtrostat and anti-PD-1 alone led to a significant decrease in blood flow in the liver compared with the vehicle control. Taken together, these findings suggested that the antitumor activity of ezurpimtrostat was enhanced by its combination with anti-PD-1.

### 3.2 PPT1 Inhibitor Combined with Anti-PD-1 Affects Tumor Growth

As illustrated in Fig. 2A, the livers of mice treated with ezurpimtrostat monotherapy or the anti-PD-1 plus ezurpimtrostat combination were similar in appearance, with smaller liver sizes and fewer macronodules than those in the control and anti-PD-1 groups. Indeed, ezurpimtrostat treatment significantly decreased liver weight and macronodule number when administered alone or in combination (Fig. 2B, C; Supplementary Table 1), whereas no significant difference was observed between the vehicle and anti-PD-1 groups. Interestingly, the number of macronodules significantly decreased when mice were treated with ezurpimtrostat in combination with anti-PD-1 compared with ezurpimtrostat alone, suggesting a benefit of the combination (Fig. 2C). Next, the variation in micronodule number and area was investigated using hematoxylin–phloxin–safron coloration of the excised liver (Fig. 2D). The combination treatment showed greater efficiency in reducing both the number (Fig. 2E) and area (Fig. 2F) of neoplastic micronodules compared with the control (Supplementary Table 1), suggesting that inhibition of PPT1 potentiates the effects of anti-PD-1 immunotherapy.

### 3.3 Local Autophagy Inhibition Facilitates T Cell Tumor Colonization and Activation

To evaluate the local action of ezurpimtrostat at the tumor level, we first evaluated two key mechanisms related to ezurpimtrostat action, inhibition of autophagy through p62 expression and inhibition of PPT1 at the tumor level. As illustrated in Fig. 3, we observed an increase in p62 ( $p = 0.0286$ ; Fig. 3A) and a decrease in PPT1 ( $p = 0.0153$ ; Fig. 3B) expression, highlighting the local action of ezurpimtrostat in inhibiting autophagy and PPT1 expression.

Next, we investigated the effects of ezurpimtrostat on the tumor cell microenvironment. As illustrated in Fig. 4A, we observed the presence of CD8<sup>+</sup> T cells at the intra- and perinodular levels. Ezurpimtrostat treatment alone or in combination increased the CD8<sup>+</sup> T cell population at the

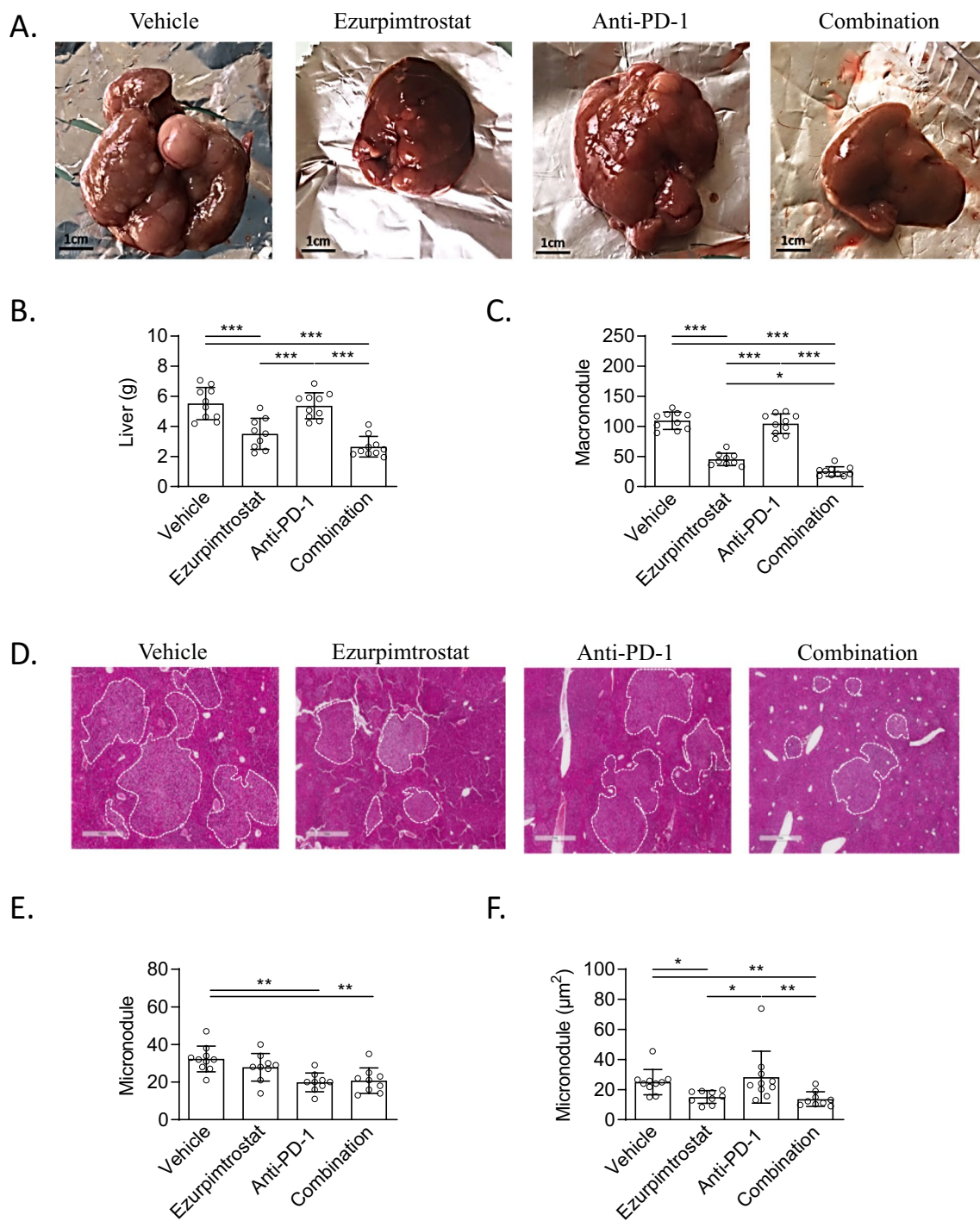


**Fig. 2** Ezurpimtrostat in combination with anti-PD-1 affects neoplastic nodules. **A** Representative pictures illustrating macroscopic livers from each group. Graph showing **B** liver weight and **C** macronodule number at the surface of the liver for each group and expressed as the mean  $\pm$  standard deviation of 10 fields. \* $p < 0.05$ , \*\*\* $p < 0.001$ .

**D** Images illustrating micronodules from the livers of each group. **E** Number and **F** area of micronodules were quantified on excised livers and expressed as the mean  $\pm$  standard deviation. \* $p < 0.05$ , \*\* $p < 0.01$

intranodular level, whereas the same population was significantly underrepresented at the perinodular level (Fig. 4B, C; Supplementary Table 1). In contrast, anti-PD-1 treatment

alone did not affect lymphocyte recruitment at either the intra- or perinodular levels. To investigate the effects of ezurpimtrostat on lymphocytes, we performed a co-culture

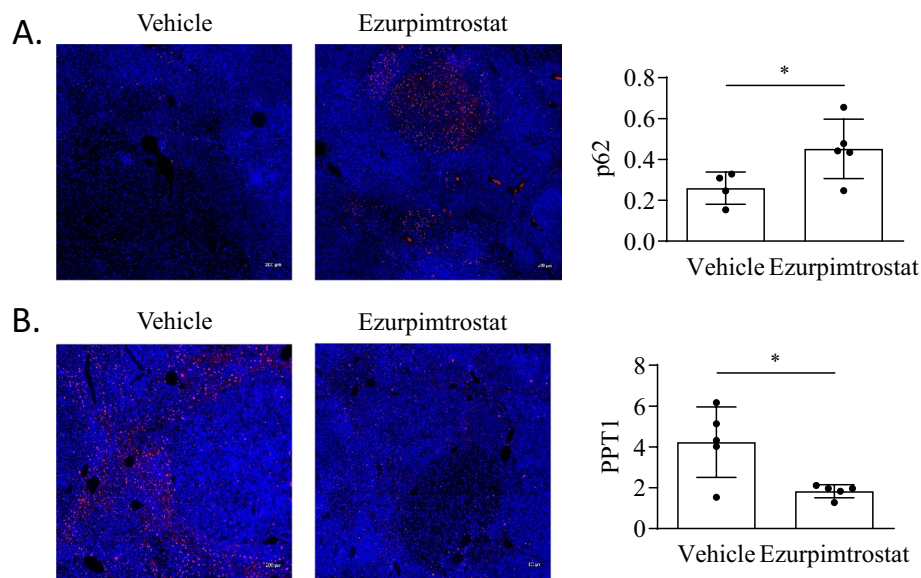


**Fig. 3** Ezurpimtrostat inhibits autophagy and PPT1 expression at the tumor level. **A** Representative pictures of p62 (red) expression and nucleus (blue) in liver biopsies from mouse treated by vehicle (left) as control or ezurpimtrostat (right); and ratio of p62 expression to cell nucleus of slides from five mice for each group using area analysis (ImageJ). Data represent the mean  $\pm$  standard deviation.  $*p < 0.05$ . **B**

Representative pictures of PPT1 (red) expression and nucleus (blue) in liver biopsies from a mouse treated by vehicle (left) as control or ezurpimtrostat (right); and ratio of PPT1 expression to cell nucleus of slides from five mice for each group using RawIntDen (ImageJ) as a measure of fluorescence intensity. Data represent the mean  $\pm$  standard deviation.  $*p < 0.05$

experiment. Interestingly, in vitro ezurpimtrostat treatment of HepG2 cells co-cultured with different lymphocyte ratios led to a decrease in cancer cell viability (Fig. 4D). To assess the immunomodulatory role of ezurpimtrostat in lymphocytes, we investigated CD8<sup>+</sup> T cell activation in co-culture experiments. Indeed, ezurpimtrostat led to a dose-dependent increase in interferon (IFN)- $\gamma$  expression by lymphocytes co-cultured with HepG2, indicating that the compound activated immune cells (Fig. 4E).

Taken together, these findings indicate that autophagy inhibition through ezurpimtrostat treatment is crucial for (1) tumor recolonization of cytotoxic CD8<sup>+</sup> lymphocytes, (2) their activation to potentiate, and (3) the antitumor activity of the compound.

### 3.4 Local Autophagy Inhibition Restores Tumor Cell MHC-I Expression

CD8<sup>+</sup> effector T cells exert antigen-specific cytotoxic effects on tumor cells by recognizing tumor antigens carried by MHC-I class I molecules [20]. Here, we report a significant increase in MHC-I protein expression in tumors from mice treated with ezurpimtrostat compared to that in the control ( $p = 0.0231$ ; Fig. 5A). Moreover, ezurpimtrostat treatment of cancer mice resulted in a positive correlation between the expression of p62, reflecting the inhibition of autophagy and MHC-I at the tumor level (Fig. 5B). No correlation was observed in the untreated control group, suggesting that

the inhibitory activity of ezurpimtrostat on the autophagy pathway is directly related to the modulation of tumor-level MHC-I protein expression. Specifically, MHC-I protein expression increased in vitro in HepG2 cells treated with ezurpimtrostat in a dose-dependent manner (Fig. 5C), highlighting the specificity of the compound for modulating MHC-I protein expression in cancer cells. In contrast, ezurpimtrostat significantly decreased in a dose-dependent manner the expression of the neighbor of BRCA1 gene 1 (NBR1) (Fig. 5D), which has been previously identified as an autophagy cargo receptor involved in the sequestration and destruction of MHC-I protein [18]. Interestingly, negative correlation was obtained between MHC-I and NBR1 expression in HepG2 treated cells ( $r = -0.65$ ,  $p = 0.039$ ) (Fig. 5E) suggesting that the restoration of MHC-I expression by ezurpimtrostat depends on NBR1.

## 4 Discussion

This study reported that PPT1 inhibition using ezurpimtrostat in combination with anti-PD-1 impairs tumor growth and significantly reduces the number of cancer macronodules in the liver, in a model in which anti-PD-1 alone does not present significant antitumor effects. The inhibition of PPT1 and the mechanisms related to autophagy potentiate the effects of anti-PD-1 immunotherapy by increasing tumor MHC-I expression, potentially allowing the recovery

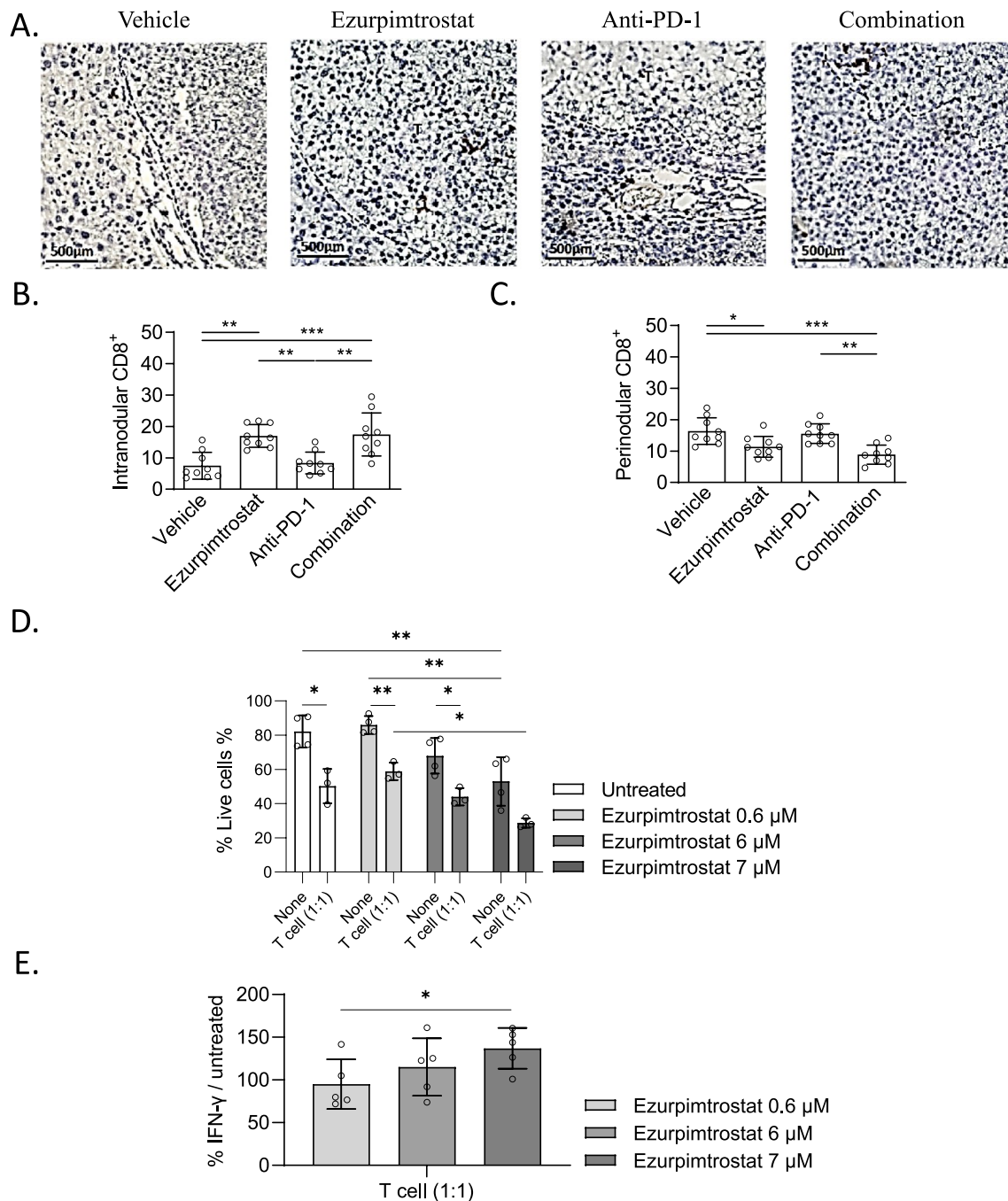


**Fig. 4** Ezurpimtrostat led to tumor MHC-I expression and immune T cell tumor colonization. **A** Representative pictures illustrating CD8<sup>+</sup> T cell population from excised liver. Quantification of CD8<sup>+</sup> T cell population at the **B** intranodular and **C** perinodular localization. Each spot represents the mean ± standard deviation of ten fields. \**p* < 0.05, \*\**p* < 0.01, \*\*\**p* < 0.001. **D** Mean fluorescence intensity of IFN-γ expressed by CD3<sup>+</sup>CD8<sup>+</sup> lymphocytes co-cultured

with cancer cell line at 0.5, 1, or 2 ratio and treated or not for 24 h by ezurpimtrostat at 0.6, 6, or 7 μM. Data represent the mean ± standard deviation. **E** Cell viability of cancer cells co-cultured or not with lymphocytes at 0.5, 1, or 2 ratio and treated or not for 24 h by GNS561 at 0.6, 6, or 7 μM. Data represent the mean ± standard deviation. \**p* < 0.05

of antigen recognition and tumor recruitment of cytotoxic CD8<sup>+</sup> lymphocytes. Autophagy is involved in immune evasion [21, 22] and promotes resistance to anti-PD-1-based therapeutic strategies/immunotherapy [23]. Our data showed

that PPT1 inhibition by ezurpimtrostat sensitizes tumors to PD-1 inhibitors. Ezurpimtrostat combined with anti-PD-1 led to T cell recolonization at the tumor site, suggesting that PPT1 inhibition counteracted immune evasion. In contrast,

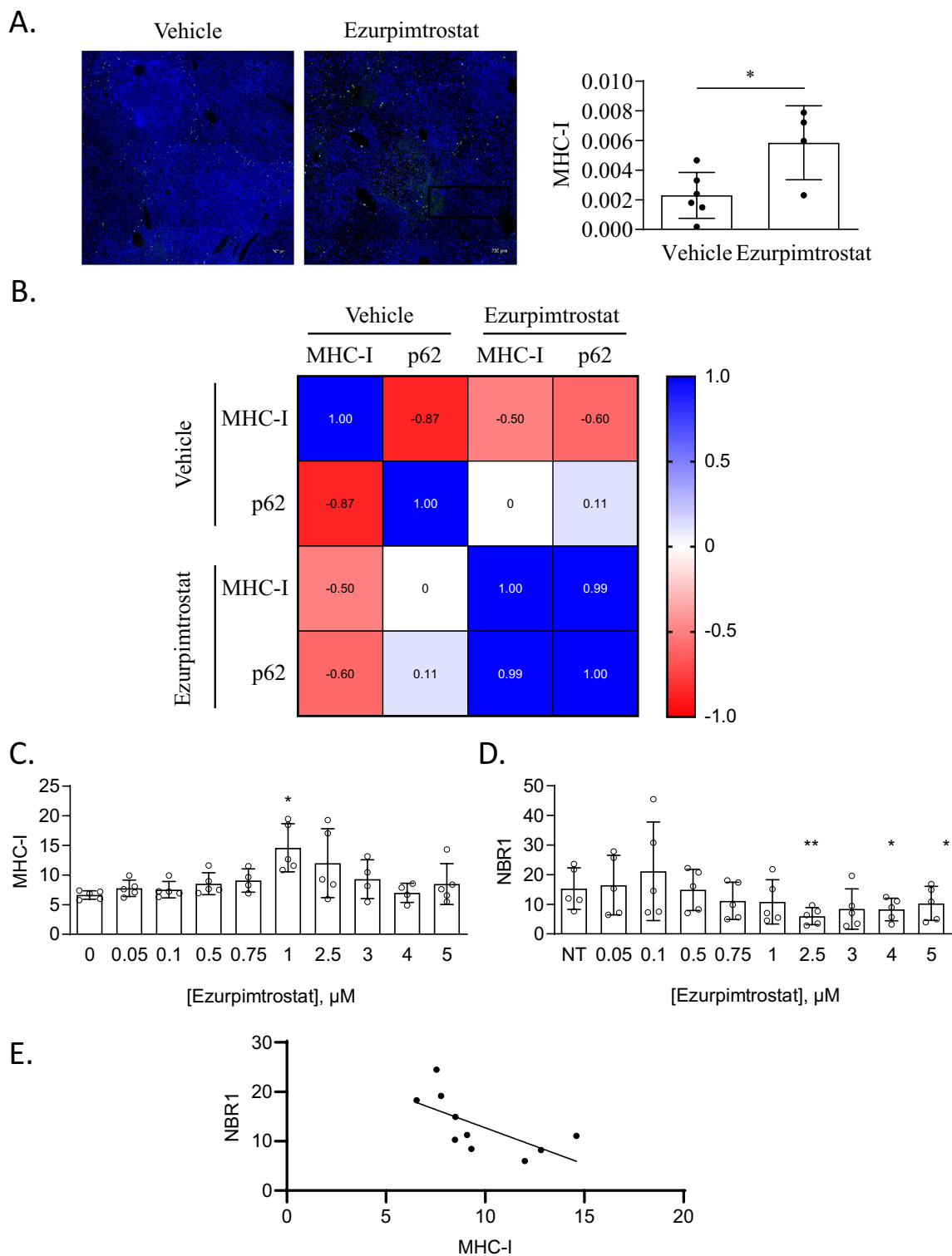


**Fig.5** Ezurpimtrostat restores MHC-I expression on cancer cells. **A** Representative pictures (left) and graph (right) of MHC-I expression (green) and nucleus (blue) in liver biopsies from a mouse treated by vehicle (left) as control or GNS561 (right). Using RawIntDen (ImageJ) as a measure of fluorescence intensity, level of expression was expressed as the ratio of MHC-I expression to cell nucleus of slides from four mice for each group. Data represent the mean  $\pm$  standard deviation. \* $p < 0.05$ . **B** Correlation matrix between MHC-I

and p62 expression from the control and GNS561 groups. Scatter dot plot illustrating the mean fluorescence intensity of **C** MHC-I and **D** NBR1 on HepG2 cell line treated or not by increase concentration of GNS561 during 24 h. Data represent the mean  $\pm$  standard deviation. \* $p < 0.05$ , \*\* $p < 0.01$ . **E** Correlation between MHC-I and NBR1 expression was investigated on HepG2 cell line treated or not by increase concentration of GNS561 during 24 h. Data represent the mean and were analyzed using the Pearson test. \* $p < 0.05$

the combination of anti-PD-1 and PPT1 inhibition with hydroxychloroquine did not modulate the number of T cells [11], suggesting that ezurpimtrostat displays immunomodulatory activity against cancer. In addition, PPT1 inhibition modulates infiltrating-CD8<sup>+</sup> T cell activation by expressing IFN- $\gamma$ , a key cytotoxic cytokine involved in the apoptosis of tumor cells [24, 25]. This finding is in accordance with the increased production of IFN- $\gamma$  by tumor-infiltrating CD8<sup>+</sup> cells observed in B16 melanoma cells and H22 tumor ascites models [26]. Interestingly, authors have reported that T cell production of IFN- $\gamma$  during chloroquine treatment was mediated by tumor-associated macrophages (TAMs). TAMs have been extensively investigated in cancer, especially their polarization into the M1 (proinflammatory) and M2 (anti-inflammatory) phenotypes [27], which exhibit antitumoral and pro-tumoral activities, respectively [28]. Sharma et al. reported that the inhibition of autophagy targeting PPT1 leads to a switch in macrophage polarization from M2 to M1 [11]. The key role of macrophage polarization switching after PPT1 inhibitor treatment has been previously reported [11, 26]. Although macrophages have been described as key immune cells involved in tumor suppression, data on their role in modulating the tumor immune microenvironment are increasing. Indeed, the switch from M2 to M1 polarization allows IFN- $\beta$  secretion by pro-inflammatory macrophages [11] as well as the tumor colonization of myeloid-derived suppressor and Treg cells [26], contributing to T cell-mediated cytotoxicity. The mechanism through which PPT1 inhibitors modulate immune cell phenotype (macrophage polarization), activation, and cytokines/chemokines remains to be explored.

The results of this study are consistent with previous reports by Yamamoto et al., which showed that the activation of CD8<sup>+</sup> T lymphocytes strongly depends on their interactions with MHC-I on the surface of tumor cells to efficiently recognize antigens [18]. Ezurpimtrostat modulated MHC-I protein expression in cancer cells in a dose-dependent manner in vitro and in vivo. The regulatory mechanisms of MHC-I and its upregulation were previously involved in the restriction of immune escape [29], and its reduction was associated with a decrease in T cell-mediated cytotoxic treatment of cancer [30]. PPT1 inhibition in pancreatic cancer models overexpresses MHC-I proteins, potentiating cancer immunotherapy [18]. In contrast, Zeng et al. reported that MHC-I protein expression decreases after PPT1 inhibition in non-small cell lung cancer cells treated with radiation therapy [31]. Moreover, the authors highlighted that MHC-I protein expression positively correlates with CD8<sup>+</sup> T cell recruitment. Interestingly, this study showed that ezurpimtrostat treatment led to tumor colonization by CD8<sup>+</sup> T cells. Other mechanisms may be involved, such as the increased expression of MHC-I on the surface of antigen-presenting cells, such as dendritic cells

after anti-autophagy drug treatment. This is involved in the promotion of the cytotoxic response of CD8<sup>+</sup> T cells during a viral immune response [32]. MHC-I is a key biomarker in cancer, as a decrease in its expression has been correlated with the worsening of prognosis [33], and mutation or loss of its heterozygosity has been implicated in resistance to immune checkpoint inhibitor therapy [34–36]. Further studies are needed to define how ezurpimtrostat treatment leads to the upregulation of MHC-I in tumor cells.

Ezurpimtrostat treatment decreases NBR1 protein expression in cancer cells. In addition to its NBR1 mRNA expression in most cancers, it is associated with low cancer specificity [37, 38]. NBR1 overexpression increases the proliferation of renal cancer cells in vitro [39] and promoted tumor metastasis in a breast cancer mouse model [40]. In contrast, the knockdown of NBR1 inhibits in vitro cell migration [41] suggesting that NBR1 is involved in cancer development. Here, we reported that ezurpimtrostat treatment leads to a decrease in NBR1 protein levels, which is consistent with previous reports by Yamamoto et al., highlighting the key role of NBR1 in immune evasion. Future studies should evaluate NBR1 as a potential therapeutic target.

Collectively, owing to its unique and original dual mechanism of action, ezurpimtrostat monotherapy in combination with anti-PD1 may represent a powerful strategy for improving T cell-mediated immunotherapies. Ezurpimtrostat-based combinations may help expand long-term clinical benefits to patients with advanced liver cancer by overcoming the elusive mechanisms of response and resistance to immune checkpoint inhibitor therapy. This strategy is currently being studied in the first-line setting of advanced hepatocellular carcinoma, in the large phase 2 trial ABE-LIVER (NCT05448677), randomizing the combination of the actual standard of care atezolizumab–bevacizumab with or without ezurpimtrostat.

**Supplementary Information** The online version contains supplementary material available at <https://doi.org/10.1007/s11523-023-01019-8>.

## Declarations

**Funding** Genoscience Pharma.

**Conflicts of Interest/Competing Interests** E.B., M.R., S.M., C.A., E.R., and P.H. are employees of Genoscience Pharma. E.R. and P.H. are shareholders of Genoscience Pharma. A.T.R. has no conflict of interest that might be relevant to the contents of this manuscript.

**Ethics Approval** All experiments were performed following Directive 2010/63/EU of the European Parliament and Council on September 22, 2010. This project was approved by the local ethic committee (Comité d'éthique en experimentation animale Lariboisière-Villemin n°9).

**Consent to Participate** Not applicable.

**Consent for Publication** All authors have approved the last version of the manuscript and its future publication.

**Availability of Data and Material** All data generated or analyzed during this study are included in this published article (and its supplementary information files).

**Code Availability** Not applicable.

**Authors' Contributions** Conception and design: EB, MR, AT-R, SM. Data analysis: EB, MR, SM. Study supervision: MR, EB, SM, PH. Writing, review of the manuscript: MR, EB, GR, TD, CA, SM, ER, PH.

## References

- Lu JY, Verkruyse LA, Hofmann SL. Lipid thioesters derived from acylated proteins accumulate in infantile neuronal ceroid lipofuscinosis: correction of the defect in lymphoblasts by recombinant palmitoyl-protein thioesterase. *Proc Natl Acad Sci USA*. 1996;93:10046–50.
- Verkruyse LA, Hofmann SL. Lysosomal targeting of palmitoyl-protein thioesterase. *J Biol Chem*. 1996;271:15831–6.
- Bagh MB, Peng S, Chandra G, Zhang Z, Singh SP, Pattabiraman N, et al. Misrouting of v-ATPase subunit V0a1 dysregulates lysosomal acidification in a neurodegenerative lysosomal storage disease model. *Nat Commun*. 2017;8:14612.
- Sancak Y, Bar-Peled L, Zoncu R, Markhard AL, Nada S, Sabatini DM. Ragulator-Rag complex targets mTORC1 to the lysosomal surface and is necessary for its activation by amino acids. *Cell*. 2010;141:290–303.
- Futai M, Sun-Wada G-H, Wada Y, Matsumoto N, Nakanishi-Matsui M. Vacuolar-type ATPase: A proton pump to lysosomal trafficking. *Proc Jpn Acad Ser B Phys Biol Sci*. 2019;95:261–77.
- Yap SQ, Mathavarajah S, Huber RJ. The converging roles of Batten disease proteins in neurodegeneration and cancer. *iScience*. 2021;24:102337.
- Rebecca VW, Nicastrì MC, Fennelly C, Chude CI, Barber-Rotenberg JS, Ronghe A, et al. PPT1 promotes tumor growth and is the molecular target of chloroquine derivatives in cancer. *Cancer Discov*. 2019;9:220–9.
- Rebecca VW, Nicastrì MC, McLaughlin N, Fennelly C, McAfee Q, Ronghe A, et al. A unified approach to targeting the lysosome's degradative and growth signaling roles. *Cancer Discov*. 2017;7:1266–83.
- Brun S, Bestion E, Raymond E, Bassissi F, Jilkova ZM, Mezouar S, et al. GNS561, a clinical-stage PPT1 inhibitor, is efficient against hepatocellular carcinoma *via* modulation of lysosomal functions. *Autophagy*. 2022;18:678–94.
- Potts MB, McMillan EA, Rosales TI, Kim HS, Ou Y-H, Toombs JE, et al. Mode of action and pharmacogenomic biomarkers for exceptional responders to didemnin B. *Nat Chem Biol*. 2015;11:401–8.
- Sharma G, Ojha R, Noguera-Ortega E, Rebecca VW, Attanasio J, Liu S, et al. PPT1 inhibition enhances the antitumor activity of anti-PD-1 antibody in melanoma. *JCI Insight*. 2020;5(17):e133225. <https://doi.org/10.1172/jci.insight.133225>.
- Wang H, Yao H, Li C, Shi H, Lan J, Li Z, et al. HIP1R targets PD-L1 to lysosomal degradation to alter T cell-mediated cytotoxicity. *Nat Chem Biol*. 2019;15:42–50.
- Mach L, Stüwe K, Hagen A, Ballaun C, Glössl J. Proteolytic processing and glycosylation of cathepsin B. The role of the primary structure of the latent precursor and of the carbohydrate moiety for cell-type-specific molecular forms of the enzyme. *Biochem J*. 1992;282:577–82.
- Harding JJ, Awada A, Roth G, Decaens T, Merle P, Kotecki N, et al. First-in-human effects of PPT1 inhibition using the oral treatment with GNS561/ezurpimtrostat in patients with primary and secondary liver cancers. *Liver Cancer*. 2022;11:268–77.
- Brun S, Bassissi F, Serdjebi C, Novello M, Tracz J, Autelitano F, et al. GNS561, a new lysosomotropic small molecule, for the treatment of intrahepatic cholangiocarcinoma. *Invest New Drugs*. 2019;37:1135–45.
- Dupuy E, Hainaud P, Villemain A, Bodevin-Phèdre E, Brouland JP, Briand P, et al. Tumoral angiogenesis and tissue factor expression during hepatocellular carcinoma progression in a transgenic mouse model. *J Hepatol*. 2003;38:793–802.
- Bonnin P, Villemain A, Vincent F, Debbabi H, Silvestre JS, Contreres JO, et al. Ultrasonic assessment of hepatic blood flow as a marker of mouse hepatocarcinoma. *Ultrasound Med Biol*. 2007;33:561–70.
- Yamamoto K, Venida A, Yano J, Biancur DE, Kakiuchi M, Gupta S, et al. Autophagy promotes immune evasion of pancreatic cancer by degrading MHC-I. *Nature*. 2020;581:100–5.
- Chen Y-W, Pan H-B, Tseng H-H, Hung Y-T, Huang J-S, Chou C-P. Assessment of blood flow in hepatocellular carcinoma: correlations of computed tomography perfusion imaging and circulating angiogenic factors. *Int J Mol Sci*. 2013;14:17536–52.
- Bian J, Lin J, Long J, Yang X, Yang X, Lu X, et al. T lymphocytes in hepatocellular carcinoma immune microenvironment: insights into human immunology and immunotherapy. *Am J Cancer Res*. 2020;10:4585–606.
- Levy JMM, Towers CG, Thorburn A. Targeting autophagy in cancer. *Nat Rev Cancer*. 2017;17:528–42.
- Mathew R, Karantza-Wadsworth V, White E. Role of autophagy in cancer. *Nat Rev Cancer*. 2007;7:961–7.
- Amaravadi RK, Yu D, Lum JJ, Bui T, Christophorou MA, Evan GI, et al. Autophagy inhibition enhances therapy-induced apoptosis in a Myc-induced model of lymphoma. *J Clin Invest*. 2007;117:326–36.
- Maimela NR, Liu S, Zhang Y. Fates of CD8<sup>+</sup> T cells in tumor microenvironment. *Comput Struct Biotechnol J*. 2019;17:1–13.
- Tau GZ, Cowan SN, Weisburg J, Braunstein NS, Rothman PB. Regulation of IFN-gamma signaling is essential for the cytotoxic activity of CD8<sup>+</sup> T cells. *J Immunol*. 2001;167:5574–82.
- Chen D, Xie J, Fiskesund R, Dong W, Liang X, Lv J, et al. Chloroquine modulates antitumor immune response by resetting tumor-associated macrophages toward M1 phenotype. *Nat Commun*. 2018;9:873.
- Mezouar S, Mege J. Changing the paradigm of IFN- $\gamma$  at the interface between innate and adaptive immunity: macrophage-derived IFN- $\gamma$ . *J Leukoc Biol*. 2020;108:419–26.
- Najafi M, Hashemi Goradel N, Farhood B, Salehi E, Nashtaei MS, Khanlarkhani N, et al. Macrophage polarity in cancer: a review. *J Cell Biochem*. 2019;120:2756–65.
- Brea EJ, Oh CY, Machado E, Budhu S, Gejman RS, Mo G, et al. Kinase regulation of human MHC Class I molecule expression on cancer cells. *Cancer Immunol Res*. 2016;4:936–47.
- Morrison BJ, Steel JC, Morris JC. Reduction of MHC-I expression limits T-lymphocyte-mediated killing of cancer-initiating cells. *BMC Cancer*. 2018;18:469.
- Zeng H, Zhang W, Gong Y, Xie C. Radiotherapy activates autophagy to increase CD8<sup>+</sup> T cell infiltration by modulating major histocompatibility complex class-I expression in non-small cell lung cancer. *J Int Med Res*. 2019;47:3818–30.
- Loi M, Müller A, Steinbach K, Niven J, Barreira da Silva R, Paul P, et al. Macroautophagy proteins control MHC Class I levels on dendritic cells and shape anti-viral CD8<sup>+</sup> T cell responses. *Cell Rep*. 2016;15:1076–87.

33. Cornel AM, Mimpen IL, Nierkens S. MHC Class I downregulation in cancer: underlying mechanisms and potential targets for cancer immunotherapy. *Cancers*. 2020;12:1760.
34. Rooney MS, Shukla SA, Wu CJ, Getz G, Hacohen N. Molecular and genetic properties of tumors associated with local immune cytolytic activity. *Cell*. 2015;160:48–61.
35. McGranahan N, Rosenthal R, Hiley CT, Rowan AJ, Watkins TBK, Wilson GA, et al. Allele-specific HLA loss and immune escape in lung cancer evolution. *Cell*. 2017;171:1259–1271.e11.
36. Rodig SJ, Gusenleitner D, Jackson DG, Gjini E, Giobbie-Hurder A, Jin C, et al. MHC proteins confer differential sensitivity to CTLA-4 and PD-1 blockade in untreated metastatic melanoma. *Sci Transl Med*. 2018;10:eaar3342.
37. Uhlen M, Zhang C, Lee S, Sjöstedt E, Fagerberg L, Bidkhori G, et al. A pathology atlas of the human cancer transcriptome. *Science*. 2017;357:eaan2507.
38. Rasmussen NL, Kournoutis A, Lamark T, Johansen T. NBR1: The archetypal selective autophagy receptor. *J Cell Biol*. 2022;221:e202208092.
39. Adolphe F, Ferlicot S, Verkarre V, Posseme K, Couvé S, Garnier P, et al. Germline mutation in the NBR1 gene involved in autophagy detected in a family with renal tumors. *Cancer Genet*. 2021;258–259:51–6.
40. Marsh T, Kenific CM, Suresh D, Gonzalez H, Shamir ER, Mei W, et al. Autophagic degradation of NBR1 restricts metastatic outgrowth during mammary tumor progression. *Dev Cell*. 2020;52:591–604.e6.
41. Kenific CM, Debnath J. NBR1-dependent selective autophagy is required for efficient cell-matrix adhesion site disassembly. *Autophagy*. 2016;12:1958–9.

Springer Nature or its licensor (e.g. a society or other partner) holds exclusive rights to this article under a publishing agreement with the author(s) or other rightsholder(s); author self-archiving of the accepted manuscript version of this article is solely governed by the terms of such publishing agreement and applicable law.